New Phytologist

Research

Control of basal jasmonate signalling and defence through modulation of intracellular cation flux capacity

Aurore Lenglet[1]*, Dawid Jaślan[2]*, Masatsugu Toyota[3,4,5], Matthias Mueller[1], Thomas Müller[2], Gerald Schönknecht[6], Irene Marten[2], Simon Gilroy[3], Rainer Hedrich[2] and Edward E. Farmer[1]

[1]Department of Plant Molecular Biology, Biophore, University of Lausanne, Lausanne CH-1015, Switzerland; [2]Institute for Molecular Plant Physiology and Biophysics, University of Würzburg, Julius-von-Sachs Platz 2, Würzburg D-97082, Germany; [3]Department of Botany, University of Wisconsin, Birge Hall, 430 Lincoln Drive, Madison, WI 53706, USA; [4]Department of Biochemistry and Molecular Biology, Saitama University, 255 Shimo-Okubo, Sakura-ku, Saitama 338-8570, Japan; [5]Japan Science and Technology Agency (JST), Precursory Research for Embryonic Science and Technology (PRESTO), Saitama 332-0012, Japan; [6]Department of Plant Biology, Ecology, and Evolution, Oklahoma State University, Stillwater, OK 74078, USA

Authors for correspondence:
Edward E. Farmer
Tel: +41 21 692 42 28
Email: edward.farmer@unil.ch

Rainer Hedrich
Tel: +49 931 31 86100
Email: hedrich@botanik.uni-wuerzburg.de

Received: *21 April 2017*
Accepted: *19 July 2017*

New Phytologist (2017)
doi: 10.1111/nph.14754

Key words: calcium, endomembrane, jasmonic acid (JA), membrane potential, two-pore channel 1 (TPC1).

Summary

- Unknown mechanisms tightly regulate the basal activity of the wound-inducible defence mediator jasmonate (JA) in undamaged tissues. However, the Arabidopsis *fatty acid oxygenation upregulated2* (*fou2*) mutant in vacuolar two-pore channel 1 ($TPC1^{D454N}$) displays high JA pathway activity in undamaged leaves. This mutant was used to explore mechanisms controlling basal JA pathway regulation.
- *fou2* was re-mutated to generate novel '*ouf*' suppressor mutants. Patch-clamping was used to examine TPC1 cation channel characteristics in the *ouf* suppressor mutants and in *fou2*. Calcium (Ca^{2+}) imaging was used to study the effects *fou2* on cytosolic Ca^{2+} concentrations.
- Six intragenic *ouf* suppressors with near wild-type (WT) JA pathway activity were recovered and one mutant, *ouf8*, affected the channel pore. At low luminal calcium concentrations, *ouf8* had little detectable effect on *fou2*. However, increased vacuolar Ca^{2+} concentrations caused channel occlusion, selectively blocking K^+ fluxes towards the cytoplasm. Cytosolic Ca^{2+} concentrations in unwounded *fou2* were found to be lower than in the unwounded WT, but they increased in a similar manner in both genotypes following wounding.
- Basal JA pathway activity can be controlled solely by manipulating endomembrane cation flux capacities. We suggest that changes in endomembrane potential affect JA pathway activity.

Introduction

Although they are wound-inducible, regulatory lipids called jasmonates (JAs) are constantly produced in undamaged plants, where their activity maintains constitutive anti-herbivore defence barriers (Howe & Jander, 2008). To do this, JAs function as potent ligands in the receptor-mediated de-repression of defence and regulatory gene transcription (Browse, 2009; Wasternack & Hause, 2013; Chini *et al.*, 2016). For example, expression of the defence gene *VEGETATIVE STORAGE PROTEIN2* (*VSP2*) is upregulated, as is the expression of regulatory *JASMONATE ZIM DOMAIN* (*JAZ*) genes such as *JAZ10*. Together, these genes provide robust markers for JA pathway activity (Acosta & Farmer, 2010). While the canonical JA signalling mechanism is increasingly well understood, there is only a rudimentary knowledge of the mechanisms controlling base-level JA pathway activity in unstimulated leaves. However, membrane depolarization following wounding has been causally linked to the activation of JA signalling in *Arabidopsis thaliana* (Mousavi *et al.*, 2013). Moreover, membrane potential changes induce JA biosynthesis and signalling necessary for prey digestion/recognition in carnivorous plants (Bemm *et al.*, 2016; Krausko *et al.*, 2017). Clearly, mutants affecting cellular ion homeostasis would be valuable tools for the study of JA pathway activation.

One such mutant is *fatty acid oxygenation upregulated2* (*fou2*) in the vacuolar cation channel two-pore channel 1 (TPC1) (Bonaventure *et al.*, 2007a). While a null allele of TPC1 had only a slight negative impact on the expression of some JA- and ethylene-regulated genes, the *fou2* gain-of-function mutant caused strong activation of the JA pathway in undamaged plants (Bonaventure *et al.*, 2007b). Transcript, protein and metabolite analyses revealed that *fou2* strikingly mimics plants being attacked by lepidopteran herbivores (Bonaventure *et al.*, 2007b). Moreover, *fou2* showed signs of potassium depletion (Bonaventure *et al.*, 2007b). Consistent with this, TPC1 is a nonselective cation channel (Hedrich & Neher, 1987; Peiter *et al.*, 2005; Gradogna *et al.*, 2009) that, when activated, provides high conductance in the vacuolar membrane (Beyhl *et al.*, 2009; Guo *et al.*, 2017). The $TPC1^{D454N}$ mutation in *fou2* affects an inhibitory luminal calcium sensor producing a hyperactive version of TPC1 that is less tightly voltage regulated as a result of its

*These authors contributed equally to this work.

increased resistance to inhibition by vacuolar calcium (Dadacz-Narloch *et al.*, 2011).

To gain insights into the mechanisms that lead to activation of the JA pathway in undamaged plants, we used a forward genetic screen in which *fou2* was re-mutated. When grown on soil under short-day conditions, juvenile-phase WT and *fou2* plants had similar morphologies. However, during entry to the adult phase, *fou2* plants began to display a characteristic visual phenotype: reduced rosette diameter, epinastic leaves and short petioles. This last trait is strongly coupled to the activation of the JA pathway (Bonaventure *et al.*, 2007a,b). Screening for reversion of *fou2* to near WT phenotypes yielded multiple '*ouf* mutants in which JA signalling was similar to that of the WT. Unique features of one of the *ouf* mutants show unequivocally that cation fluxes from the vacuole act as a powerful trigger of JA pathway activation. This finding was extended using reverse genetic approaches.

Materials and Methods

Plants, growth conditions and genetic screen

T-DNA insertion lines were obtained from the Nottingham Arabidopsis Stock Center (NASC). *Arabidopsis thaliana* (L.) Heynh Columbia (Col) was the WT and the background for *tpc1-2* SALK_145413 (At4g03560 *fou2* ($TPC1^{D454N}$); Bonaventure *et al.*, 2007b). The *fou2* mutant was ethyl methanesulphonate-mutagenized and putative revertant mutants, named '*ouf*, were scored visually. Selection and backcrossing of the *ouf* mutants are described in Supporting Information Methods S1 and S2, Notes S1. Plants were grown on soil at 70% humidity under light and temperature conditions depending on the application. Plants illuminated with 100 $\mu mol\ m^{-2}\ s^{-1}$ photosynthetically available radiation for 10 h at 21°C were used for reverse transcriptase–quantitative polymerase chain reaction (RT-qPCR), fatty acid oxygenation assay and phenotype characterization (see Methods S3). For electrophysiological measurements and determination of TPC1 transcripts (see Methods S4), plants were cultivated under a day : night regime of 8 h : 16 h with a light intensity of 150 $\mu mol\ m^{-2}\ s^{-1}$ and a temperature of 22°C : 16°C. Long-day conditions (14 h : 10 h, light : darkness; 21°C) or continuous day conditions (24 h light; 21°C) were used to examine flowering phenotypes.

Electrophysiology

The patch-clamp technique was applied to vacuoles liberated from mesophyll protoplasts of 4- to 5-wk-old plants essentially as described previously (Beyhl *et al.*, 2009). Current recordings were carried out with the cytoplasmic side of the vacuolar membrane facing the bath medium. In whole-vacuole measurements, the standard bath solution facing the cytosolic side of the vacuolar membrane contained 150 mM KCl and 10 mM Hepes (pH 7.5/Tris). Because of its stimulatory effect (Hedrich & Neher, 1987; Beyhl *et al.*, 2009) the bath medium was loaded with high Ca^{2+} (1 mM) to provide for high TPC1 channel activity and macroscopic current amplitudes for resolving potential effects of the different mutations on TPC1 channel features. The standard pipette solution at the vacuolar side of the whole vacuole membrane consisted of 150 mM KCl, 2 mM $MgCl_2$, 10 mM Hepes (pH 7.5/Tris) and 0.1 mM EGTA (no $CaCl_2$ added). In some patch-clamp experiments (as indicated in the legends to Figs 2 and 3), the pipette solution contained 10 mM $CaCl_2$ instead of 0.1 mM EGTA. For single channel recordings, the bath medium contained 100 mM KCl, 0.5 mM $CaCl_2$ and 10 mM Hepes (pH 7.5/Tris) while the pipette medium was composed of 100 mM KCl, 2 mM $MgCl_2$ and 2 mM EGTA and adjusted to pH 5.5 with 10 mM MES/Tris. All patch-clamp solutions were adjusted to an osmolality of 500 $mOsmol\ kg^{-1}$ using D-sorbitol. In response to voltage pulses in the range of −80 to +110 mV applied in 10-mV steps from a holding voltage of −60 mV, macroscopic currents were usually recorded with a sampling rate of 100 µs at a low-pass filter frequency of 2.9 kHz. Electrophysiology methods and measurements are further described in Methods S5.

Insect bioassays

Insect assays are described in Methods S6.

Yellow cameleon-Nano 65 (YCNano-65) Förster resonance energy transfer (FRET) sensor, ratiometric Ca^{2+} imaging and statistics

In order to obtain the $TPC1^{D454N}$ (*fou2*) line expressing the YCNano-65 FRET sensor, a plasmid containing the 35S:: YCNano-65 FRET sensor construct (Choi *et al.*, 2014) was introduced into *fou2* using *Agrobacterium tumefasciens* floral dip. The transformed plants were isolated by BASTA (Bayer Crop Science, Monheim am Rhein, Germany) selection combined with a PCR analysis (see Methods S7). Plants expressing the YCNano-65 FRET sensor were imaged with a motorized fluorescence stereo microscope (SMZ-25; Nikon Instruments Inc., Melville, NY, USA) equipped with a ×1 objective lens (P2-SHR PLAN APO; Nikon Instruments Inc.), image splitting optics (W-VIEW GEMINI; Hamamatsu Corp., Bridgewater, NJ, USA) and a sCMOS camera (ORCA-Flash4.0 V2; Hamamatsu Corp.). YCNano-65 was excited using a mercury lamp (motorized Intensilight Hg Illuminator; Nikon Instruments Inc.), a 436/20-nm excitation filter (ET436/20x; Chroma Technology Corp., Bellows Falls, VT, USA) and a 455-nm dichroic mirror (T455lp; Chroma Technology Corp.). The fluorescent signal was separated by a 515-nm dichroic mirror (T515lp; Chroma Technology Corp.) installed in the W-VIEW GEMINI and the resultant cyan fluorescent protein (CFP) (460–500 nm) and FRET-dependent cpVenus (520–540 nm) emission independently passed through 480/40-nm and 535/30-nm filters, respectively (ET480/40 m and ET535/30 m; Chroma Technology Corp.). A pair of the CFP and FRET images was simultaneously acquired every 4 s with the sCMOS camera using the NIS-Elements imaging software (Nikon Instruments Inc.). The FRET : CFP ratio was calculated using the 6D imaging and Ratio and FRET plug-in modules (Nikon Instruments Inc.). Statistical methods are described in Methods S8.

Results

ouf mutants

fou2 was re-mutagenized and M2 plants were scored visually, searching for restoration to near-WT phenotypes. Initially, eight putative revertants were isolated and named *ouf1* to *ouf8*. Two of these mutants (*ouf4* and *ouf5*) were eliminated after backcrossing, as they were not fully penetrant. The remaining *ouf* mutants were placed in three morphological classes where class I was the closest to WT, and class III had the most divergent morphology (Fig. S1). After reaching backcross 1 (BC1F2) and ensuring that the *ouf* phenotypes were stable, we proceeded to characterize the mutants. *fou2* (Bonaventure *et al.*, 2007a) was originally selected with an assay for enhanced lipoxygenase activity (Caldelari & Farmer, 1998). Using this assay, we found near-WT fatty acid oxygenation activity in all *ouf* mutants (Fig. 1a). Furthermore, *fou2* shows high levels of activity of the JA pathway including constitutively high expression of the JA-regulated *VSP2* gene (Bonaventure *et al.*, 2007a). Basal and wound-induced *VSP2* levels were assessed in the *ouf* mutants and were similar to those of the WT (Fig. 1b). Similar results were obtained with the JA-controlled *JAZ10* gene (Fig. S2a,b). Additionally, *TPC1* transcripts were detected in the *ouf* mutants (Fig. S2c).

As the null allele *tpc1-2* displays a near-WT rosette phenotype and does not strongly impact JA-regulated gene expression (Bonaventure *et al.*, 2007a,b), we tested the possibility that the re-mutagenesis of *fou2* had introduced further mutations into the *TPC1* gene. Fig. 1(c) shows the results of sequencing *TPC1* in the *ouf* mutants. *ouf1* and *ouf3* displayed different single base pair deletions (g1586− and g1587−, respectively) that both lead to Trp529 being replaced by a stop codon (W529X). Of these two mutants, only *ouf1* was further analysed. For *ouf2*, we found a new allele (g1748a) predicted to change Gly583 to aspartate in the luminal part of transmembrane domain S11, between the voltage sensor (transmembrane domain 10; Dadacz-Narloch *et al.*, 2011; Guo *et al.*, 2016; Kintzer & Stroud, 2016) and the pore. *ouf6* was a missense mutation of Ala669 to valine in transmembrane domain 12, close the C-terminal end of the TPC1 channel. *ouf7* carried a non-sense mutation that introduces a stop codon at amino acid position 492. In *ouf8*, a missense mutation changed Met629 to isoleucine, potentially affecting the channel pore.

Channel activity of *tpc1* mutants

Mutants were analysed with the patch-clamp technique and compared with *fou2* and WT. When the whole-vacuole configuration was established on mesophyll vacuoles under symmetrical 150 mM potassium, pronounced macroscopic time-dependent outward currents from WT and *fou2* vacuoles were evoked upon depolarizing voltage pulses (Fig. 2a). By contrast, TPC1 outward currents were not elicited upon depolarization in *ouf1*, *ouf2* and *ouf7* mutant lines as in the TPC1 loss-of-function mutant *tpc1-2* (Fig. S3). However, both the *ouf6* and *ouf8* mutant lines exhibited fast current activation as for $TPC1^{D454N}$ in *fou2* (Figs S3, S4). TPC1 current density was strongly reduced in *ouf6* compared with *fou2*, for example at +110 mV by 80% (Fig. 2a,b). Such a decrease in whole-vacuole current densities can be caused

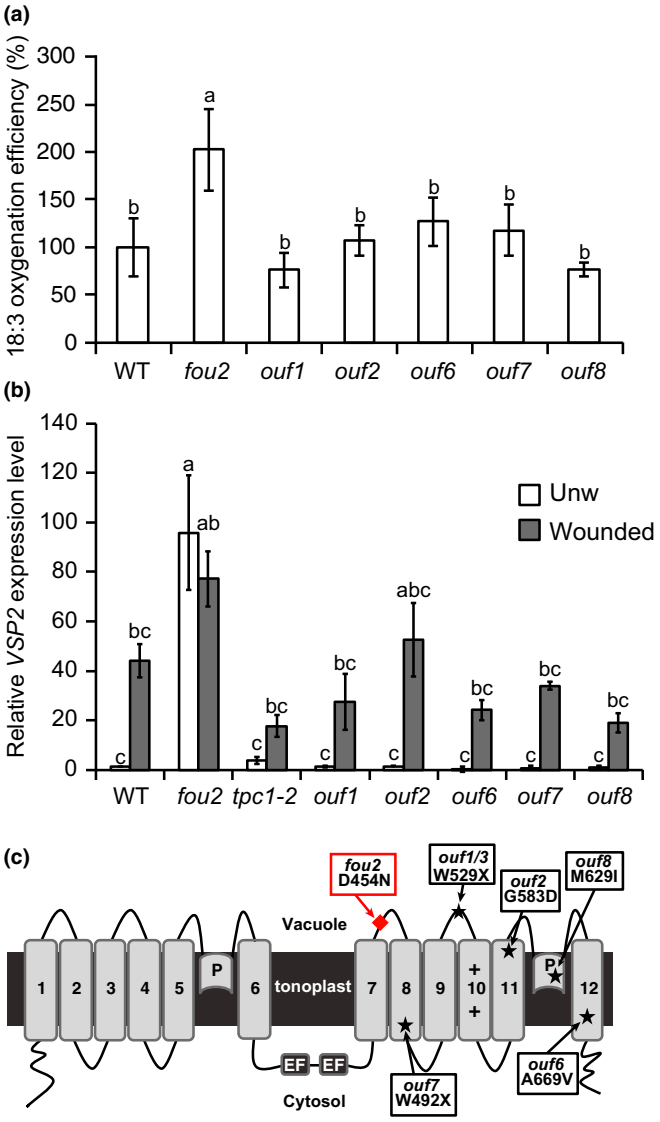

Fig. 1 Initial characterization of *fou2 suppressor* (*ouf*) mutants. (a) *In vitro* fatty acid oxygenation catalysed by *Arabidopsis thaliana* leaf extracts. Juice from leaf 8 (2 µl) of 4-wk-old plants was incubated in the presence of 1-[^{14}C] α-linolenic acid (18:3) for 2 min. After extraction and thin-layer chromatography, radioactivity in 18:3 oxidation products was quantified. The 18:3 oxidation level catalysed by wild-type (WT) leaf juice was set at 100%. Mean ± SD of three independent biological replicates are shown. Letters indicate statistically significant differences as determined by Tukey's honest significant difference (HSD) test at $P = 9.55^{e-11}$. (b) Quantitative RT-PCR of *VEGETATIVE STORAGE PROTEIN2* (*VSP2*) transcripts in unwounded (unw) plants (leaf 8) or 1 h after wounding leaf 8. *VSP2* transcripts were normalized to those of *UBIQUITIN-CONJUGATING ENZYME21* (*UBQ21*) and are displayed relative to the expression in the WT control. Mean ± SEM of four combined experiment with three biological replicates each are shown. Letters indicate statistically significant differences with a *P*-value = 1.4^{e-10} as determined by Tukey's HSD test. (c) Localization and predicted amino acid modifications in the *ouf* mutants are indicated on the two-pore channel 1 (TPC1) monomer by the black stars. Red diamond, *fou2* mutation; EF, cytosolic EF-hands; +, voltage sensor. All mutations affect the C-half of the protein.

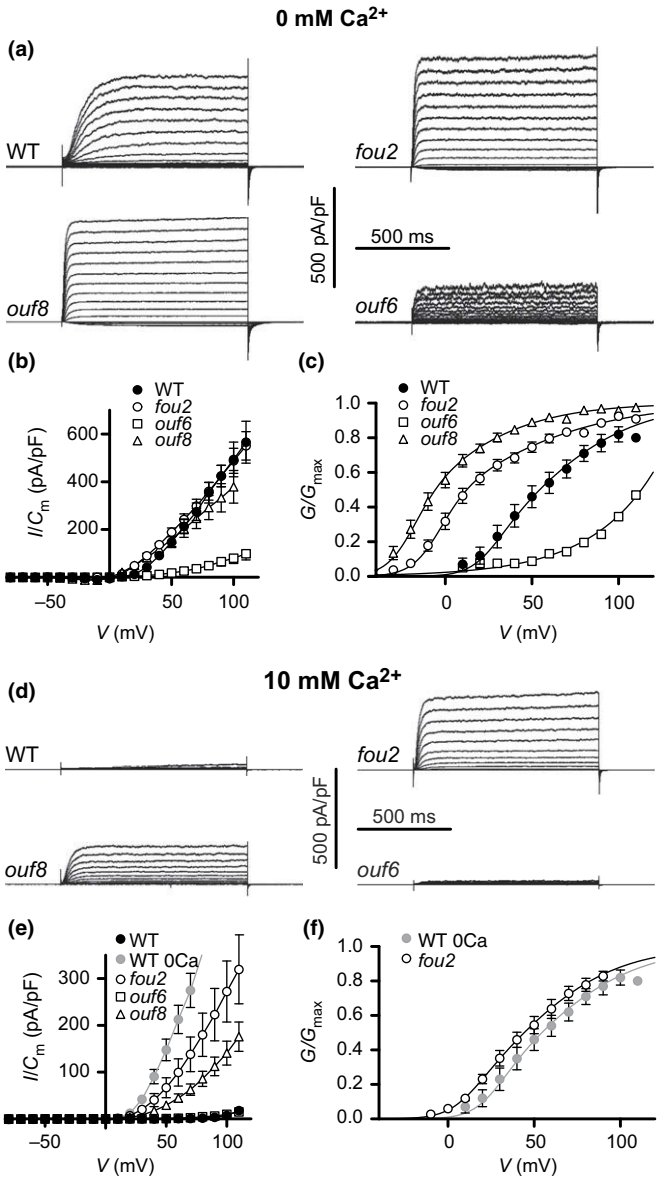

Fig. 2 Voltage-dependent channel activity of two-pore channel 1 (TPC1) mutants. Macroscopic current recordings (a, d), current–voltage curves (I/C_m in pA/pF; b, e), and macroscopic conductance–voltage curves (G/G_{max}; c, f) of wild-type (WT) *Arabidopsis thaliana*, *fatty acid oxygenation upregulated2* (*fou2*), *ouf6*, and *ouf8* in the absence (a–c) and presence (d–f) of 10 mM luminal Ca^{2+} are shown. In (b) and (e), data points are connected for clarity. Macroscopic conductance–voltage curves (G/G_{max}) were estimated from tail current measurements in the absence (c) or presence (f) of 10 mM luminal Ca^{2+} except for 'WT 0Ca' (closed grey circles) where the measurements were performed in the absence of luminal Ca^{2+}. Lines in (c) and (f) represent fits of the data points with a double-Boltzmann distribution (Pottosin *et al.*, 2004; Dadacz-Narloch *et al.*, 2011) with values for V_1, V_2, z_1 and z_2, as summarized in Supporting Information Table S1. Data points in (b, c, e, f) are the mean ± SEM of three to five replicates.

by reduced channel density, a lower single-channel conductance and/or fewer open channels. To resolve this, we determined normalized conductance–voltage curves (G/G_{max}) from tail current experiments (Fig. 2c) as a measure of relative voltage-dependent open-channel probability of TPC1 (Dadacz-Narloch *et al.*, 2011). As reported earlier (Bonaventure *et al.*, 2007a; Beyhl *et al.*, 2009), *fou2* channels exhibit conductance–voltage curves that are shifted to negative membrane voltages compared with WT. In comparison, the *ouf6* mutation shifted the conductance–voltage curves to the positive voltage range (Fig. 2c; Table S1), and therefore TPC1 channel activity was strongly reduced in *ouf6*. Surprisingly, given the near-WT JA responses seen in *ouf8*, whole-vacuole outward current densities of this mutant and *fou2* were comparable (Fig. 2b). Conductance–voltage curves deduced from tail current experiments revealed that *ouf8* voltage dependence was shifted in a *fou2*-like fashion towards negative membrane potentials (Fig. 2c; Table S1).

ouf8 pore occlusion by vacuolar Ca^{2+}

Patch-clamp results presented so far were obtained in the absence of vacuolar Ca^{2+} because, in contrast to WT, *fou2* has been shown to be largely insensitive to vacuolar Ca^{2+} (Dadacz-Narloch *et al.*, 2011; Guo *et al.*, 2017), and the reverting mutations A669V in *ouf6* and M629I in *ouf8* are not expected to affect the luminal calcium sensor because of their distant locations from the sensor. Nevertheless, we could not exclude the possibility that luminal Ca^{2+} might affect the revertants. To explore this, we studied the response of *ouf8*, *ouf6*, *fou2* and WT to 10 mM luminal Ca^{2+}. At high luminal Ca^{2+}, outward currents for WT and *ouf6* largely disappeared (Fig. 2d,e). By contrast, *fou2* and *ouf8* still displayed substantial voltage-dependent outward currents (Fig. 2d,e). With 10 mM vacuolar Ca^{2+}, whole-vacuole currents for *fou2* were about twice as large as *ouf8* currents. For *fou2*, where conductance–voltage curves could be estimated in the presence of 10 mM vacuolar Ca^{2+}, voltage-dependent open probabilities were comparable to WT open probabilities in the absence of vacuolar Ca^{2+} (Fig. 2f).

As an estimate of channel density, we calculated the maximum possible current densities that would be expected if all TPC1 channels were open (Fig. 3a). Comparable current densities were obtained for WT and *fou2*. By contrast, *ouf6* and *ouf8* vacuoles displayed lower current densities. While *ouf6* current densities saturated at positive voltages, WT, *fou2*, and *ouf8* current densities displayed a linear (ohmic) current–voltage relationship (Fig. 3a). To determine whether smaller possible maximum currents for *ouf6* and *ouf8* reflect reduced single channel conductance, or reduced channel density, single channel conductance was determined (Fig. 3b,c). Single TPC1 channel fluctuations were recorded from WT, *fou2*, *ouf6* and *ouf8* in membrane patches with the cytoplasmic side of the vacuole membrane orientated to the bath medium (Fig. 3b). These fluctuations were not observed with the *tpc1-2* DNA insertion mutant. TPC1 channels from WT and *fou2* lines had comparable single channel conductance at positive membrane potentials (Fig. 3b,c), as previously shown at negative voltages (Dadacz-Narloch *et al.*, 2011). By contrast, TPC1 channels in *ouf6* and *ouf8* had smaller single channel current amplitudes (Fig. 3b), and thus lower ion transport capacities. A plot of single-channel current amplitudes against applied voltages revealed a single channel conductance for both revertants that was only about half that of WT and *fou2*

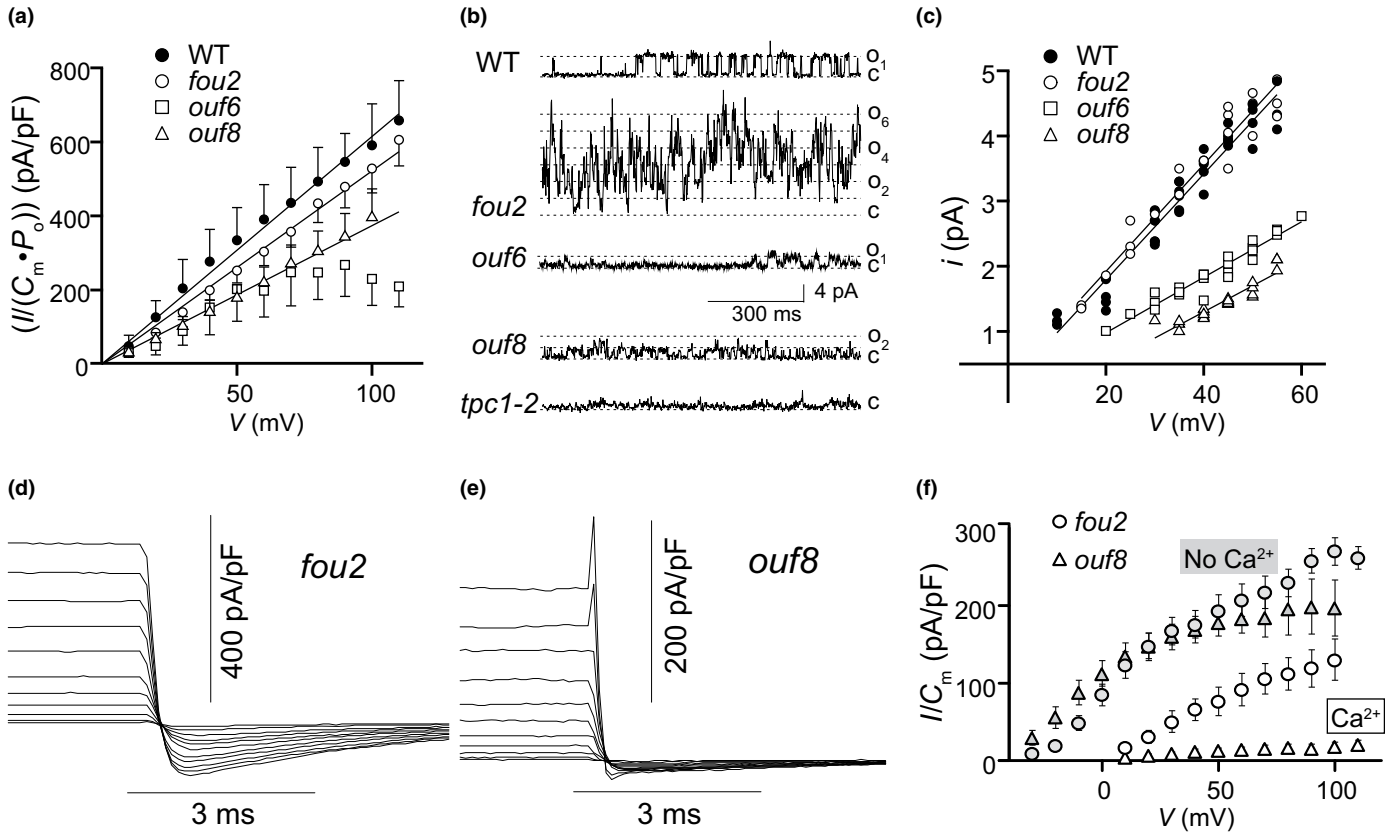

Fig. 3 Current density, single-channel conductance and effect of luminal Ca^{2+} on two-pore channel 1 (TPC1) tail currents from wild-type (WT) *Arabidopsis thaliana*, *fatty acid oxygenation upregulated2* (*fou2*), *ouf6*, and *ouf8* vacuoles. (a) To compare TPC1 current densities for different mutant lines, we estimated current amplitudes that would be expected if all TPC1 channels were open. Recorded whole-vacuole current densities (I/C_m in pA/pF) were divided by relative open channel probability (P_o) derived from normalized conductance–voltage curves (G/G_{max}) to calculate maximum possible current densities ($I/(C_m \cdot P_o)$ in pA/pF). These estimated maximum possible current densities are shown as the mean ± SEM of three to five replicates. Data sets from WT, *fou2* and *ouf8* were fitted by linear regression, to emphasize the expected linear (i.e. ohmic) current–voltage relationship. (b) Single channel fluctuations monitored at +45 mV from excised membrane patches of WT, *fou2*, *ouf6*, *ouf8* and *tpc1-2* vacuoles. The current level *C* indicates where all channels are closed, while O_1, O_2, O_3, . . ., O_n identify the current levels where 1, 2, 3, . . ., *n* channels are open, respectively. (c) Single-channel current amplitudes (*i* in pA) determined from all-point histograms are plotted against the corresponding membrane voltages. Data points derived from four to six replicates (*n*) for each mutant were fitted on linear regression lines. From the slope of the lines, the following single-channel conductance γ values were deduced: $\gamma_{WT} = 81$ pS ($n = 6$); $\gamma_{fou2} = 82$ pS ($n = 4$); $\gamma_{ouf6} = 43$ pS ($n = 4$) and $\gamma_{ouf8} = 40$ pS ($n = 5$). Experiments were performed with 0.5 mM Ca^{2+} at the cytosolic side of the vacuole membrane in the absence of Ca^{2+} in the vacuole lumen. (d, e) Tail current analysis for *fou2* and *ouf8* vacuoles at high temporal resolution. Jumping from different clamp voltages (−80 to +110 mV in 10-mV increments) to −60 mV evoked instantaneous inward tail currents, which relaxed within 10–20 ms. Capacitive transients were compensated by comparing transient currents at the onset and the end of each voltage pulse. Compared with *fou2*, in *ouf8* tail currents are largely absent in the presence of 10 mM luminal Ca^{2+}. Note that the scaling of current densities (*y*-axis) differs by a factor of 2, to compensate for different single-channel conductance. (f) Tail current densities (I/C_m in pA/pF) of *fou2* (circles) and *ouf8* (triangles) vacuoles in the absence (grey symbols) and presence of 10 mM luminal Ca^{2+}. The mean ± SEM for four to seven replicates is shown.

(Fig. 3c). This substantiates the conclusion that TPC1 channel densities were comparable in vacuolar membranes from WT, *fou2*, *ouf6*, and *ouf8*. Finally, tail currents were measured at negative membrane potentials to gain insights into the effect of luminal Ca^{2+} on cation release by TPC1 from the vacuole into the cytosol. This experiment yielded striking results. While *fou2* displayed tail currents in the presence or absence of 10 mM Ca^{2+}, tail currents for *ouf8* were largely reduced at high luminal Ca^{2+}, in particular in the negative voltage range (Figs 3d–f, S5). Nevertheless, *fou2* and *ouf8* tail currents exhibited a similar outward-rectifying voltage dependence under high luminal Ca^{2+} (Fig. S5). Thus, while TPC1-mediated cation import into the vacuole seems to be comparable for *fou2* and *ouf8*, cation release from the vacuole into the cytosol was strongly reduced in *ouf8*. The unique features of *ouf8* then led us to explore its defence capacity.

ouf8 reduces the elevated defence capacity of *fou2*

In comparison to *fou2*, *ouf8* restored near-WT JA-regulated *VSP2* defence gene expression (Fig. 1b). How does this relate to defence? We examined the ability of *fou2* and *ouf8* to restrict the growth of lepidopteran larvae. The assays (Fig. 4) revealed that *fou2* had a high defence capacity, whereas insects gained similar weight on *tpc1-2*, *ouf8* and the WT. Additionally, larval survival was lower on *fou2* than on the three other genotypes tested.

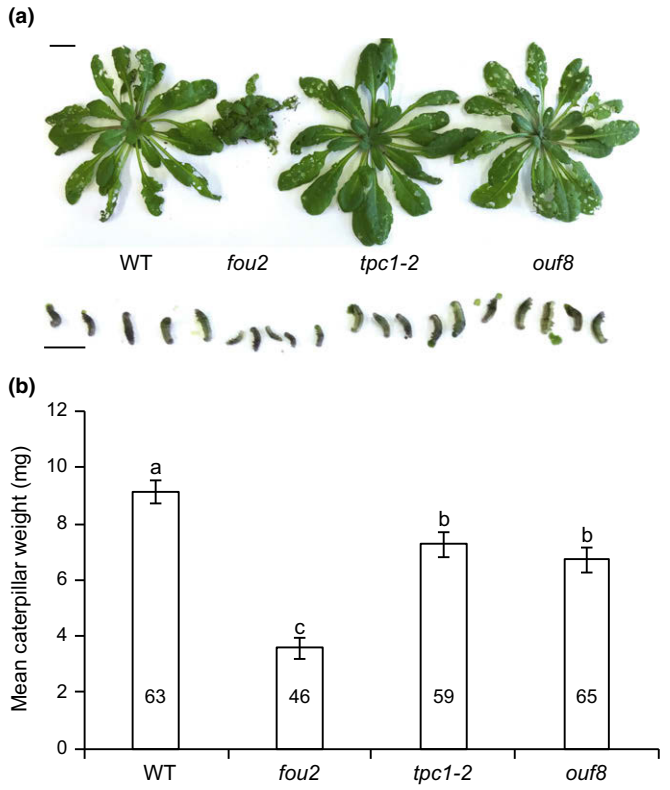

Fig. 4 *Spodoptera littoralis* weight gain on *ouf8* versus *fatty acid oxygenation upregulated2* (*fou2*). Neonate *S. littoralis* larvae were placed on 5-wk-old *Arabidopsis thaliana* plants (six larvae per plant; 11 plants) and allowed to feed for 11 d. (a) Rosette and insect morphology after feeding. Bars: plants (1 cm); insects (0.5 cm). (b) *Spodoptera littoralis* mass after feeding. Error bars, ± SEM. Letters indicate significant differences at $P = 1.03^{e-13}$ as determined by Tukey's honest significant difference (HSD) test. Numbers within boxes indicate how many larvae survived. Similar results were obtained in three independent experiments.

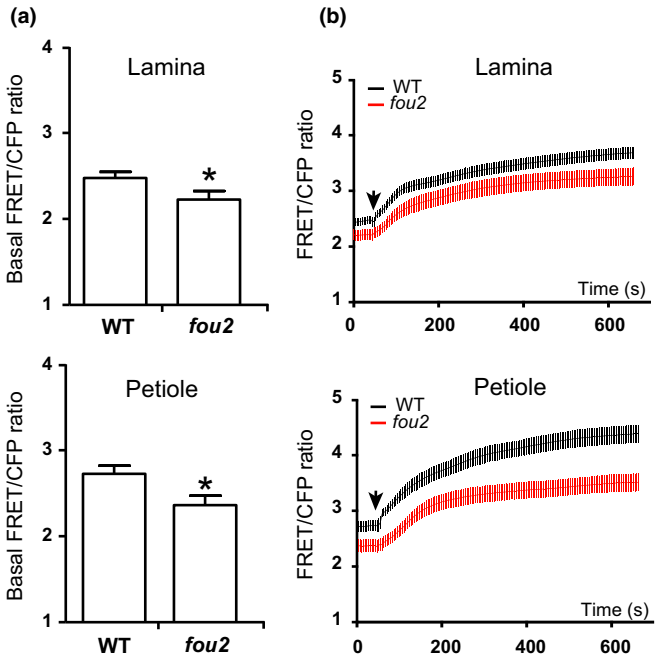

Fig. 5 Cytoplasmic calcium (Ca^{2+}) concentrations in wild-type (WT) and *fatty acid oxygenation upregulated2* (*fou2*). (a) Basal Ca^{2+} concentration (Förster resonance energy transfer (FRET) : cyan fluorescent protein (CFP) ratio) in WT *Arabidopsis thaliana* and *fou2* lamina (upper panel) and petiole (lower panel). Basal FRET:CFP ratios were calculated before cutting the leaf tip. The mean ± SEM of 20 biological replicates are shown. Statistical analysis (*t*-test): *, $P < 0.05$. (b) Wound-induced cytoplasmic Ca^{2+} changes in WT and *fou2* lamina (upper panel) and petiole (lower panel). Black line, WT; red line, *fou2*. Arrows, 40% of the leaf tip was cut with scissors at *c*. 40 s. FRET:CFP images were acquired every 4 s. Mean ± SEM of 20 biological replicates are shown.

Cytosolic calcium measurement in *fou2*

Previous work (Bonaventure *et al.*, 2007b; Beyhl *et al.*, 2009) and the present patch-clamp data are consistent with a role of potassium (K^+) fluxes in basal JA pathway activity. However, fluxes of protons or cations such as Ca^{2+} might also affect this process. Indeed, *fou2* has a vacuolar Ca^{2+} content approx. 1.6-fold higher than the WT (Beyhl *et al.*, 2009) and the possibility that high cytosolic Ca^{2+} activates JA synthesis has been proposed (Beyhl *et al.*, 2009). To test this, we analysed cytosolic Ca^{2+} concentrations using the FRET-based Ca^{2+} indicator YCNano-65 (Choi *et al.*, 2014). This revealed that cytoplasmic Ca^{2+} was actually lower in unwounded *fou2* than in the unwounded WT (Fig. 5a), but Ca^{2+} concentrations increased with similar kinetics in response to wounding in both genotypes (Figs 5b, S6).

Discussion

The precise regulation of defence pathway activity throughout the plant life-cycle is essential, as investment in defence can strongly impact plant growth (Huot *et al.*, 2014). To investigate how basal JA pathway activity is regulated, we previously performed a genetic screen for mutants with highly active JA pathways in undamaged plants. The screen identified *fou2*, a gain-of-function mutant in the voltage-gated cation channel TPC1 (Bonaventure *et al.*, 2007a). The $TPC1^{D454N}$ mutation in *fou2* creates a hyperactive channel that activates JA signalling in undamaged plants (Bonaventure *et al.*, 2007a). A remarkable feature of this mutant is that basal activity of the JA pathway is high and yet *fou2* still responds to wounding (Bonaventure *et al.*, 2007a,b and Figs 1b, S2a,b). The *fou2* mutant therefore provides a unique tool with which to study JA activation in unwounded plants using an ion channel with an unequivocal intracellular localization. Furthermore, the electrophysiological properties of TPC1 can be studied in its native membrane environment.

To gain further insights into base-level JA pathway regulation, we focussed further effort on *fou2*. Using forward genetics, novel suppressors of *fou2* were isolated. From the outset, *ouf8* proved to be the most interesting because it affected the channel pore region and could therefore provide insights into how the *fou2* mutation activates JA signalling. This novel mutant reduced the unitary conductance of *fou2* and also gave rise to an enhanced voltage-dependent blockade of the ion pathway when luminal Ca^{2+} concentrations were high. This observation further confirms that Ca^{2+} can enter the TPC1 pore region and hinder K^+ permeation (Pottosin *et al.*, 2004; Gradogna *et al.*, 2009). As a result of

this Ca^{2+} block, the *ouf8* mutation strongly impaired inward (vacuole-to-cytosol) K^+ currents in patch-clamp experiments and rescued the WT phenotype in the living plant. These findings provide evidence that the cation transport capacity of $TPC1^{D454N}$ activates JA synthesis. When cation release from the vacuole is strongly reduced in the *ouf8* mutant, JA pathway activity is similar to that of the WT and the *tpc1-2* null mutant. Consistent with this, we found that the level of anti-lepidopteran defence in *fou2* was high, but that of *ouf8* was similar to that of *tpc1-2*. These results suggest that the selective modulation of endomembrane ion flux capacities can be used to manipulate a plant's investment in defence before attack.

How might *ouf8* affect the TPC1 pore? In the crystal structure of AtTPC1 (Guo *et al.*, 2016; Kintzer & Stroud, 2016), which reflects the closed conformation, the rectangular-shaped pore opening measures 7.7 by 9.1 Å at the cytoplasmic entry (distance between the CO atoms of Met629 and Thr264, respectively). This large opening, and the fact that the side chain of Met629 does not occlude the pore, suggests that the altered ion conductivity in *ouf8* is probably not attributable to an altered pore size. Met629 was recently found to be part of selectivity filter II in TPC1 (Guo *et al.*, 2017). The Met629Ile mutation in *ouf8* might alter the arrangement of the carbonyl groups, thereby affecting ion dehydration/rehydration. Indeed, the arrangement of backbone carbonyl groups lining the pore somewhat resembles the selectivity filters of cation channels, for example of the K^+ channel from *Streptomyces lividans* and high-affinity potassium transporter family, in which the carbonyl groups facilitate ion selectivity by mimicking the hydration shell for the transported ions (Zhou *et al.*, 2001; Dudev & Lim, 2010).

TPC1s are complex, dimeric ion channels that are conserved in plants and animals. How human TPC1 (hTPC1) functions is a subject of controversy (Morgan & Galione, 2014), but similarities between AtTPC1 and hTPC1 are such that the plant channel has been used as a scaffold for the production of hybrid TPC1 channels to investigate channel selectivity (Guo *et al.*, 2017). Permeable to monovalent and divalent cations such as K^+ and Ca^{2+} (Pottosin *et al.*, 2001; Guo *et al.*, 2017), AtTPC1 is regulated by luminal Ca^{2+} (inhibitory), cytosolic Ca^{2+} (activating) and luminal pH (Peiter *et al.*, 2005; Beyhl *et al.*, 2009; Dadacz-Narloch *et al.*, 2011). How does the action of $TPC1^{D454N}$ (*fou2*) lead to JA pathway activation? Here we consider two nonexclusive scenarios; they involve Ca^{2+} and membrane potential. Cytosolic Ca^{2+} increases are characteristic of wounded plants (Kiep *et al.*, 2015) and impact JA signalling (Yang *et al.*, 2012; Matschi *et al.*, 2013; Scholz *et al.*, 2014). Additionally, previous pharmacological studies of cytosolic Ca^{2+} increases in tomato (*Solanum lycopersicum*) cells treated with the peptide elicitor systemin provided evidence for Ca^{2+} release from both extracellular and intracellular stores (Moyen *et al.*, 1998). We found that, while vacuoles in *fou2* have higher-than-WT luminal Ca^{2+} concentrations (Beyhl *et al.*, 2009), this mutant has slightly lower basal cytosolic Ca^{2+} than the WT. Cytosolic Ca^{2+} increases after wounding were similar in the two plants (Fig. 5b). At this point, our results provide no evidence that global increases in cytosolic Ca^{2+} concentration in resting (unwounded) *fou2* underlie the increased basal activity of the JA pathway in this plant. We leave open the possibilities that either highly localized Ca^{2+} signatures or endomembrane Ca^{2+} uptake leads (indirectly) to activation of the JA pathway.

A related possibility is that $TPC1^{D454N}$ may affect leaf cell endomembrane potentials through its high, inwardly rectifying (luminal to cytosol) K^+ and Ca^{2+} permeability. This hypothesis is attractive as hTPC1 is a Ca^{2+}- and proton-regulated cation channel (Lagostena *et al.*, 2017) that acts to control membrane potential in endolysosomal compartments (Cang *et al.*, 2014). AtTPC1 is regulated in a similar manner (Peiter *et al.*, 2005; Beyhl *et al.*, 2009; Dadacz-Narloch *et al.*, 2011; Guo *et al.*, 2017), and therefore a similar function is plausible. Strikingly, several published studies are consistent with a link between membrane potential and activation of JA synthesis. For example, strong membrane depolarizations that powerfully activate the JA pathway are triggered by current injection into healthy Arabidopsis leaves (Mousavi *et al.*, 2013). Also in Arabidopsis, the reduced activity of a Golgi-expressed V-H^+-ATPase that may contribute to maintaining membrane potential caused the accumulation of 12-oxophytodienoic acid (OPDA), a precursor of JA (Brüx *et al.*, 2008). Finally, nigericin and gramicidin, agents that dissipate H^+ and monovalent ion gradients, strongly stimulated the expression of JA-regulated genes in tomato (Schaller & Frasson, 2001).

A parsimonious interpretation of our results is that the *fou2* channel variant ($TPC1^{D454N}$) depolarizes endomembranes by increasing cation fluxes towards the cytosol. When elevated cation release into the cytosol in *fou2* is blocked by the secondary *ouf8* mutation, then the activation of the JA pathway seen in *fou2* is suppressed as well. What does this tell us about the control of JA pathway activity in the WT plant? Our results provide rigorous genetic and biophysical evidence that cation fluxes across endomembranes help to control basal JA pathway activity in undamaged vegetative tissues. Furthermore, it is likely that the mechanisms controlling JA pathway activity in undamaged plants converge with those that control its activity upon wounding. It is therefore possible that endomembrane-associated ion fluxes also participate centrally to control JA pathway activity in leaves distal to severe wounds.

Acknowledgements

We thank S. Kellenberger (Lausanne) and N. Geldner (Lausanne) for critical discussion, and K. Trageser (Wuerzburg) for help with acquisition of single-channel raw data. This work was supported by grants from JST PRESTO to M.T., the National Science Foundation (MCB1329723) to S.G., the Deutsche Forschungsgemeinschaft (FOR964) to R.H. and Swiss National Science Foundation grants (31003A-155960, 31003A-138235 and CRSII3 154438) to E.E.F.

Author contributions

A.L., I.M., R.H. and E.E.F. designed the research; A.L., D.J., M.M. and M.T. performed experiments; A.L., D.J., M.T., T.M., G.S. and S.G. analysed results; E.E.F., R.H., I.M., A.L., D.J., T.M. and G.S. wrote the manuscript.

References

Acosta I, Farmer EE. 2010. Jasmonates. *The Arabidopsis Book* (*American Society of Plant Biologists*) **8**: e0129.

Bemm F, Becker D, Larish C, Kreuzer I, Escalante-Perez M, Schulze WX, Ankenbrand M, Van de Weyer A-L, Krol E, Al-Rasheid KA *et al.* 2016. Venus flytrap carnivorous lifestyle builds on herbivore defense strategies. *Genome Research* **26**: 812–825.

Beyhl D, Hörtensteiner S, Martinoia E, Farmer EE, Fromm J, Marten I, Hedrich R. 2009. The *fou2* mutation in the major vacuolar cation channel TPC1 confers tolerance to inhibitory luminal calcium. *Plant Journal* **58**: 715–723.

Bonaventure G, Gfeller A, Proebsting WM, Hörtensteiner S, Chételat A, Martinoia E, Farmer EE. 2007a. A gain-of-function allele of TPC1 activates oxylipin biogenesis after leaf wounding in *Arabidopsis*. *Plant Journal* **49**: 889–898.

Bonaventure G, Gfeller A, Rodríguez VM, Armand F, Farmer EE. 2007b. The *fou2* gain-of-function allele and the wild-type allele of two pore channel 1 contribute to different extents or by different mechanisms to defense gene expression in *Arabidopsis*. *Plant Cell Physiology* **48**: 1775–1789.

Browse J. 2009. Jasmonate passes muster: a receptor and targets for the defense hormone. *Annual Review of Plant Biology* **60**: 183–205.

Brüx A, Liu T-Y, Krebs M, Stierhof Y-D, Lohmann JU, Miersch O, Wasternack C, Schumacher K. 2008. Reduced V-ATPase activity in the trans-Golgi network causes oxylipin-dependent hypocotyl growth inhibition in Arabidopsis. *Plant Cell* **20**: 1088–1100.

Caldelari D, Farmer EE. 1998. A rapid assay for the coupled cell free generation of oxylipins. *Phytochemistry* **47**: 599–604.

Cang C, Bekele B, Ren D. 2014. The voltage-gated sodium channel TPC1 confers endolysosomal excitability. *Nature Chemical Biology* **10**: 463–469.

Chini A, Gimenez-Ibanez S, Goossens A, Solano R. 2016. Redundancy and specificity in jasmonate signalling. *Current Opinion in Plant Biology* **33**: 147–156.

Choi W-G, Toyota M, Kim S-H, Hilleary R, Gilroy S. 2014. Salt stress-induced Ca^{2+} waves are associated with rapid, long-distance root-to-shoot signaling in plants. *Proceedings of the National Academy of Sciences, USA* **111**: 6497–6502.

Dadacz-Narloch B, Beyhl D, Larish C, López-Sanjurjo EJ, Reski R, Kuchitsu K, Müller TD, Schönknecht G, Hedrich R. 2011. A novel calcium binding site in the slow vacuolar cation channel TPC1 senses luminal calcium levels. *Plant Cell* **23**: 2696–2707.

Dudev T, Lim C. 2010. Factors governing the Na^+ vs K^+ selectivity in sodium ion channels. *Journal of the American Chemical Society* **132**: 2321–2332.

Gradogna A, Scholz-Starke J, Gutla PV, Carpaneto A. 2009. Fluorescence combined with excised patch: measuring calcium currents in plant cation channels. *Plant Journal* **58**: 175–182.

Guo J, Zeng W, Chen Q, Lee C, Chen L, Yang Y, Cang C, Ren D, Jiang Y. 2016. Structure of the voltage-gated two-pore channel TPC1 from *Arabidopsis thaliana*. *Nature* **531**: 196–201.

Guo J, Zeng W, Jiang Y. 2017. Tuning the ion selectivity of two-pore channels. *Proceedings of the National Academy of Sciences, USA* **114**: 1009–1014.

Hedrich R, Neher E. 1987. Cytoplasmic calcium regulates voltage-dependent ion channels in plant vacuoles. *Nature* **329**: 833–836.

Howe GA, Jander G. 2008. Plant immunity to insect herbivores. *Annual Review of Plant Biology* **59**: 41–66.

Huot B, Yao J, Montgomery BL, He SY. 2014. Growth-defense tradeoffs in plants: a balancing act to optimize fitness. *Molecular Plant* **7**: 1267–1287.

Kiep V, Vadassery J, Lattke J, Maaß JP, Boland W, Peiter E, Mithöfer A. 2015. Systemic cytosolic Ca^{2+} elevation is activated upon wounding and herbivory in *Arabidopsis*. *New Phytologist* **207**: 996–1004.

Kintzer A, Stroud RM. 2016. Structure, inhibition, and regulation of two-pore channel TPC1 from *Arabidopsis thaliana*. *Nature* **531**: 258–264.

Krausko M, Perutka Z, Šebela M, Šamajová O, Šamaj J, Novák O, Pavlovič A. 2017. The role of electrical and jasmonate signalling in the recognition of captured prey in the carnivorous sundew plant *Drosera capensis*. *New Phytologist* **213**: 1818–1835.

Lagostena L, Festa M, Pusch M, Carpaneto A. 2017. The human two-pore channel 1 is modulated by cytosolic and luminal calcium. *Scientific Reports* **7**: 439000.

Matschi S, Werner S, Schulze WX, Legen J, Hilger HH, Romeis T. 2013. Function of calcium-dependent protein kinase CPK28 of *Arabidopsis thaliana* in plant stem elongation and vascular development. *Plant Journal* **73**: 883–896.

Morgan AJ, Galione A. 2014. Two-pore channels (TPCs): current controversies. *BioEssays* **36**: 173–183.

Mousavi SAR, Chauvin A, Pascaud F, Kellenberger S, Farmer EE. 2013. *GLUTAMATE RECEPTOR-LIKE* genes mediate leaf-to-leaf wound signalling. *Nature* **500**: 422–426.

Moyen C, Jones J, Knight MR, Johannes E. 1998. Systemin triggers an increase of cytoplasmic calcium in tomato mesophyll cells: Ca2 + mobilization from intra- and extracellular compartments. *Plant, Cell & Environment* **21**: 1101–1111.

Peiter E, Maathuis FJM, Mills LN, Knight H, Pelloux J, Hetherington AM, Sanders D. 2005. The vacuolar Ca^{2+}-activated channel TPC1 regulates germination and stomatal movement. *Nature* **434**: 404–408.

Pottosin II, Dobrovinskaya OR, Muniz J. 2001. Conduction of monovalent and divalent cations in the slow vacuolar channel. *Journal of Membrane Biology* **181**: 55–65.

Pottosin II, Martínez-Estévez M, Dobrovinskaya OR, Muñíz JS, Schönknecht G. 2004. Mechanism of luminal Ca^{2+} and Mg^{2+} action on the vacuolar slowly activating channels. *Planta* **219**: 1057–1070.

Schaller A, Frasson D. 2001. Introduction of wound response gene expression in tomato leaves by ionophores. *Planta* **212**: 431–435.

Scholz SS, Vadassery J, Heyer M, Reichelt M, Bender KW, Snedden WA, Boland W, Mithöfer A. 2014. Mutation of the Arabidopsis calmodulin-like protein CML37 deregulates the jasmonate pathway and enhances susceptibility to herbivory. *Molecular Plant* **7**: 1712–1726.

Wasternack C, Hause B. 2013. Jasmonates: biosynthesis, perception, signal transduction and action in plant stress response, growth and development. An update to the 2007 review in Annals of Botany. *Annals of Botany* **111**: 1021–1058.

Yang D-H, Hettenhausen C, Baldwin IT, Wu J. 2012. Silencing *Nicotiana attenuata* calcium-dependent protein kinases, CDPK4 and CDPK5, strongly up-regulates wound- and hervivory-induced jasmonic acid accumulations. *Plant Physiology* **159**: 1591–1607.

Zhou Y, Morais-Cabral JH, Kaufman A, MacKinnon R. 2001. Chemistry of ion coordination and hydration revealed by a K^+ channel-Fab complex at 2.0 Å resolution. *Nature* **414**: 43–48.

Supporting Information

Additional Supporting Information may be found online in the Supporting Information tab for this article:

Fig. S1 Phenotype of *ouf* mutants.

Fig. S2 *JAZ10* and *TPC1* expression in *ouf* mutants.

Fig. S3 Macroscopic current recordings from different TPC1 channel variants.

Fig. S4 Half-activation times of TPC1 channel variants.

Fig. S5 Voltage-dependent Ca^{2+} block of *ouf8* and *fou2* channels.

Fig. S6 Real-time imaging of the cytosolic Ca^{2+} changes in WT and *fou2* leaf upon wounding.

Table S1 Voltage-dependent gating parameters

Methods S1 Plant material and growth conditions.

Methods S2 Mutagenesis, selection and backcrossing.

Methods S3 Fatty acid oxygenation assays.

Methods S4 Genotyping, sequencing and gene expression analyses.

Methods S5 Electrophysiology.

Methods S6 Insect bioassays.

Methods S7 Generation of plants expressing the FRET-based Ca^{2+} indication Yellow Cameleon-Nano 65.

Methods S8 Statistical analysis.

Notes S1 References for the Supporting Information.

Please note: Wiley Blackwell are not responsible for the content or functionality of any Supporting Information supplied by the authors. Any queries (other than missing material) should be directed to the *New Phytologist* Central Office.